Global and Planetary Change 185 (2020) 103089

Contents lists available at ScienceDirect

Global and Planetary Change

journal homepage: www.elsevier.com/locate/gloplacha

Research article

Paleomagnetic constraints on the early Miocene closure of the southern Neo-Tethys (Van region; East Anatolia): Inferences for the timing of Eurasia-Arabia collision

Erhan Gülyüz[a,*], Hülya Durak[a], Murat Özkaptan[b], Wout Krijgsman[c]

[a] Van Yüzüncü Yıl University, Department of Geological Engineering, Van, Turkey
[b] Karadeniz Technical University, Department of Geophysical Engineering, Trabzon, Turkey
[c] Utrecht University, Department of Earth Sciences, 3584 CD Utrecht, the Netherlands

ARTICLE INFO

Keywords:
Neo-Tethys
Arabian-Eurasia collision
Magnetostratigraphy
AMS
Eastern Anatolia

ABSTRACT

Oligocene-Miocene convergence of the Eurasian and Arabian plates resulted in (i) the gradual closure of the Neo-Tethys Ocean that formed an open marine connection between the Indian Ocean and the proto-Mediterranean until the early Miocene and (ii) Eurasia-Arabia continental collision. Remnants of the Neo-Tethys basin are found scattered over eastern Anatolia. The Van region of SE Anatolia contains a unique stratigraphic succession (Van Formation) of this ancient marine corridor, showing a gradual transition from deep-marine marls to continental clastics and shallow marine deposits. This formation is considered a key unit for the late stage evolution of the Neo-Tethys Ocean as it contains one of the youngest marine deposits of the southern Neo-Tethys branch in SE Anatolia. Here, we present new magnetostratigraphic and Anisotropy of Magnetic Susceptibility (AMS) data to better constrain the timing of the marine-continental transition and the style of deformation in the Van region. The Van Formation was sampled in ~2-m stratigraphic resolution, with ~350 paleomagnetic cores drilled in stratigraphic order. These cores were analyzed with thermal and alternating field demagnetization, resulting in a magnetic polarity pattern that could straightforwardly be correlated to the standard Geomagnetic Polarity Time Scale (GPTS). The base of the section has an age of ~19.5 Ma, the marine-continental transition is dated at 18.8 Ma, and the top of the succession has an age of ~16.8 Ma. The AMS data show a conspicuous change from extensional to contractional patterns, coinciding with the end of open marine environments, at an age of ~19 Ma. We hypothesize that the closure of the marine basin and the concomitant change in stress regime in the Van region are related to the onset of Eurasia-Arabia collision and the terminal subduction of the Neo-Tethys oceanic lithosphere.

1. Introduction

Plate tectonic processes, causing continental collision and closure of ancient ocean basins and sea straits, play a major role in Earth's dynamics. These processes result in the formation of large mountain ranges and create a change in faunal migration styles from marine gateways to continental corridors. Quantitative tools to date the collision and closure process are essential to understand the pace and mode of the corresponding regional tectonic and paleoenvironmental transformations and the potentially global palaeoclimatological variations. Responses of continental collision may be expressed in the sedimentological records of the associated foreland basins, and state-of-the-art dating techniques like radio-isotopic dating and magnetostratigraphy may help unravelling the deformational history in time and space.

The E-W trending Neo-Tethys Ocean evolved between the Eurasian, Arabian and African plates and formed a vast marine domain extending from the present-day Mediterranean Sea to the Indian Ocean. It comprised two marine branches which remnants are presently found in Anatolia; a northern branch at the boundary between the Pontide (Eurasia) and Tauride-Anatolide (Africa) blocks, represented by the İzmir-Ankara-Erzincan suture zone (İAESZ), and a southern branch between the Tauride-Anatolide block and the Arabian platform (e.g. Şengör and Yılmaz, 1981; Yılmaz, 1993) (Fig. 1).

Africa-Europe convergence during the Cretaceous to Miocene, with a north-dipping subduction setting, progressively closed the Neo-Tethys Ocean and formed the SE Anatolian high plateau. Closure of the southern Neo-Tethys branch gave way to (i) a break in the connection between the proto-Mediterranean Sea and Indian Ocean, (ii) a shift in

* Corresponding author.
E-mail address: gulyuzerhan@gmail.com (E. Gülyüz).

https://doi.org/10.1016/j.gloplacha.2019.103089
Received 30 May 2019; Received in revised form 26 November 2019; Accepted 26 November 2019
Available online 28 November 2019
0921-8181/

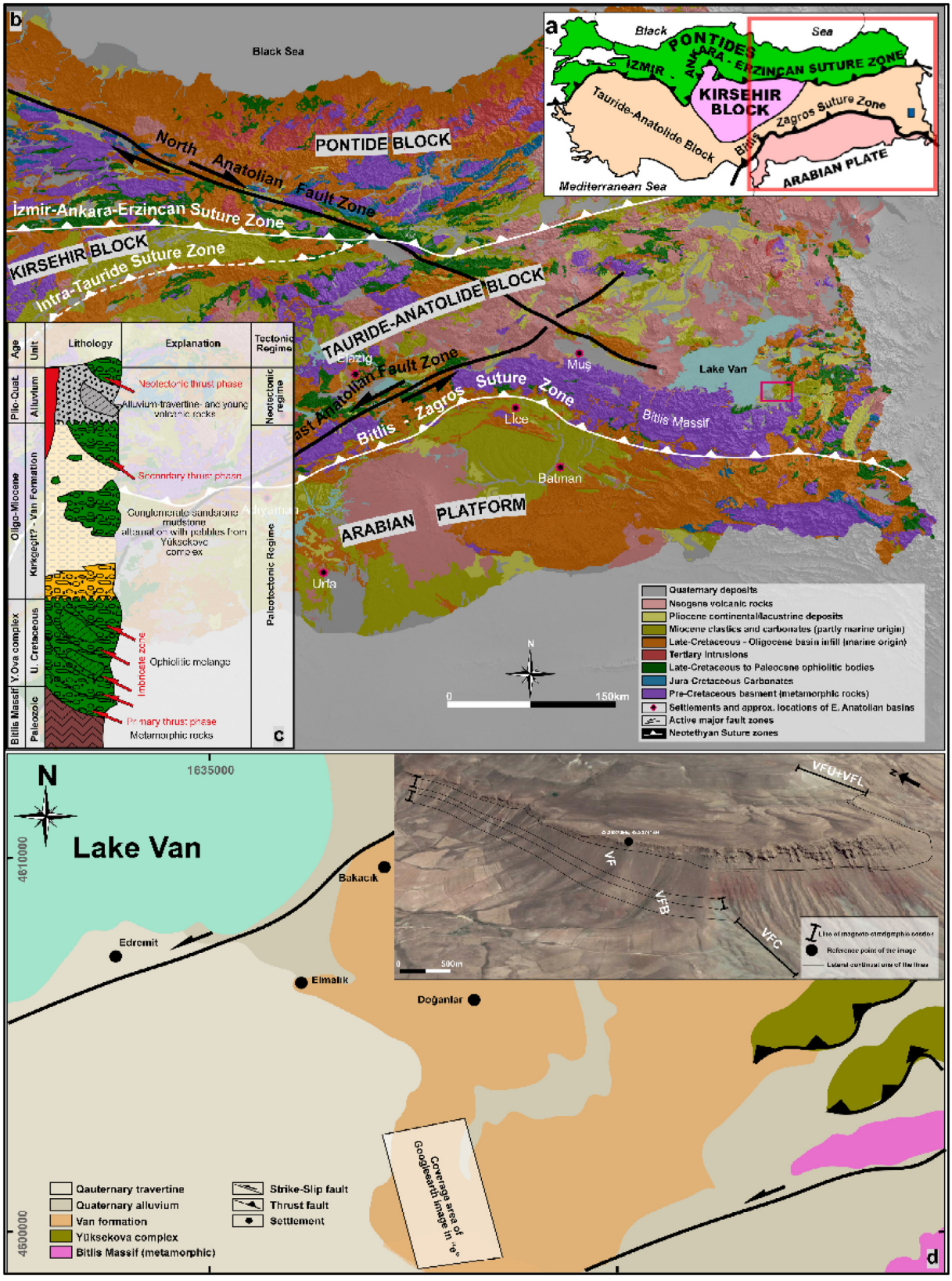

Fig. 1. a) Major tectonic zones of Anatolia (modified after Görür et al., 1984). b) Geological map of Eastern Anatolia (modified from the MTA 2002 map). c) Tectono-stratigraphic section of Eastern Anatolia (modified after Koçyiğit 2013). d) Geological map of the study area. Red rectangle in "B" shows the location of the study area and Google Earth image in "D" shows the location of the magnetostratigraphic sampling trajectory. (For interpretation of the references to colour in this figure legend, the reader is referred to the web version of this article.)

deformation styles and the initiation of a compressional regime (beginning of the still active tectonic period) on the overriding Anatolian Plate, and (iii) a change in magmatism from subduction related arc magmatism to collision – post-collision magmatism.

The exact timing of both the soft-intermediate suturing stage and the hard collision stage of the continental blocks are still on debate (Allen and Armstrong, 2008; Darin et al., 2018; Keskin, 2003; Koshnaw et al., 2019; Okay et al., 2010; Yılmaz, 1993; Zhang et al., 2017). Studies dealing with crystalline rocks give a wide age range for both soft and hard collision phases. Low temperature studies on the magmatic units of the active Eurasian margin indicate pre-Oligocene (> 34 Ma) uplift/exhumation of the region (Karaoğlan et al., 2016). Fission track ages of basement rocks suggest that the metamorphic massifs of SE-Anatolia started to exhume around 20–11 Ma (Cavazza et al., 2018; Okay et al., 2010). Based on fission track and apatite helium dating from the Sivas Basin, ages of 40–45 Ma and 20 Ma are proposed for the soft and hard collision events along the Bitlis Zagros Suture Zone (BZSZ), respectively (Darin et al., 2018). An age of 27 Ma for the collision initiation age was derived from predictions on ophiolite consumption and shortening rate calculations related to the subduction-collision system of the Zagros part (McQuarrie and Van Hinsbergen, 2013). A study of red bed sequences exposed on the Arabian foreland, provided U−Pb zircon ages inferring that the consumption of Neo-Tethys crust and Arabia-Eurasia continental collision took place after 26 Ma (Koshnaw et al., 2019). Ages of 23–20 Ma, gathered from subduction to *syn*-collisional type granitoids located at the north of the BZSZ, are also interpreted as time constraints for the collision (Açlan and Duruk, 2018; Oyan, 2018). Geochemical studies on the collision associated magmatic rocks of SE Anatolia revealed collisional and post-collisional signatures younger than 13 Ma (Ercan et al., 1990; Keskin, 2003; Keskin et al., 1998; Oyan et al., 2016; Özdemir and Güleç, 2014; Özdemir et al., 2019; Pearce et al., 1990). The sedimentary records of the Muş, Elazığ and Maraş basins suggested an early Tortonian age (~11 Ma) for the continental collision event (Hüsing et al., 2009). Finally, a sediment provenance analyses study, determining both Eurasian and Arabian sources in late Miocene clastics, suggested an age between 11 and 5 Ma for the collision event in SW Iran (Zhang et al., 2017).

In this paper we aim to create an unequivocal tectono-stratigraphic model for the progressive collision evolution process by studying the sedimentary sequences of the southern branch of the Neo-Tethys that comprise the time interval of continental collision. We selected the Van Formation in SE Anatolia as key sedimentary sequence as this unit comprises a complete succession of deep marine, continental and shallow marine Miocene deposits. The location on the active Eurasian margin, combined with the stratigraphic development of the Van Formation, provide a unique opportunity to determine the timing of the collision event in Eastern Anatolia because the transition from deep marine marls to continental deposits reflects the commencement of uplift and the docking of the continents. We aim to precisely date the paleoenvironmental changes in the Van Formation by magnetostratigraphic tools to better constrain the timing of depositional styles in the basin. Additionally, we focus on the Anisotropy of Magnetic Susceptibility (AMS) of the dated sedimentary sequences. AMS patterns are thought to represent tectonic strain and may reflect changes in deformation style throughout the formation. A precisely dated sedimentary succession that represents the Neo-Tethys closure is thus crucial for brightening the blur in the different geological records and debatable evolutionary scenarios about the tectonic history of SE Anatolia.

2. Geological setting

The basement rocks of SE Anatolia comprise magmatic (mainly granitoids), ophiolitic (the Yüksekova Mélange) and metamorphic (the Bitlis Massif) rocks that have a Cretaceous/pre-Cretaceous emplacement age (Fig. 1). They all predate the latest stage of the Eurasia-Arabia convergence system. On the other hand, Cenozoic sedimentary rocks, together with their magmatic equivalents, are considered as products of the convergence system. The sedimentary rocks are, based on the tectonic periods during which they were deposited, grouped in two (Koçyiğit, 2013; Koçyiğit et al., 2001); (i) Oligocene-Miocene marine units deposited before the continental collision of the Arabian and Anatolian plates and, (ii) Mio-Pliocene to Quaternary continental units deposited after the collision (Fig. 1c). An angular relationship between these two units supports this division in the Van region as well. The youngest Miocene units in SE-Anatolia are interpreted as fore-land basin deposits (Hüsing et al., 2009) and they are considered the most suitable sequences to record the late stage evolution of the southern branch of the Neotethys Ocean because foreland infills are considered as the final products of subduction-collision systems.

The Van Formation, the main subject of this study, is located ~100 km to the north of the promontory thrust of the collision zone (Bitlis-Zagros) (Fig. 1b) and pre-defined foreland deposits. It comprises early-middle Miocene deep to shallow marine sequences (Demirci, 2016; Sağlam, 2003) that were deposited in the northernmost extend of the Mediterranean-Indian Ocean gateway. Although numerous Miocene basins exist on the SE-Anatolian part of the Eurasian Plate (e.g. Muş, Elazıg, and Malatya located at 1500–2200 m altitudes) and on the northern promontory of the Arabian plate (e.g. Batman, Adıyaman, Lice and Urfa foreland basins located at 500–700 m altitudes) (Fig. 1b), their distribution shows a rather fragmented pattern. Fragmentation is mainly controlled by the uplift of the Bitlis massif during continental collision, volcanism and strike-slip tectonism, which makes the Neogene paleogeographic evolution of the Neo-Tethys hard to reconstruct.

The Van formation is one of the best places in Eastern Anatolia to constrain the timing of the collision event. In contrast to foreland deposits of the subduction-collision system, the sedimentary sequences of the Van Formation have the potential to record the responses of the initial collision-related uplift events, because the region is located on the active margin of the subduction-collision system. This margin may have started to uplift by docking of the continents. In addition, the Van formation is one of the most extensive and undeformed units in the region, which allows to magnetostratigraphically date the subduction-collision event.

2.1. Depositional setting of the Van Formation

The ~400 m thick (maximum observable thickness) Miocene Van Formation is subdivided in three members. Transitions are sharp and are, from bottom to top, determined by; (i) greenish mudstone-sandstone alternations, (ii) red sandstones and conglomerates and (iii) beige-yellow fossiliferous grainstone-sandstone alternations (Figs. 2 and 3). The first member is dominated by monotonous, thick (> 20 m) mudstones with thin (< 20 cm) discontinuous sandstone beds. Depositional environments are mainly represented by low-energy settings, although re-worked benthic fossils (corals) and some turbidites (with parts of Bouma sequences) are found. The second member mainly contains red mudstone-sandstone-conglomerate alternations, showing trough-like geometries and discontinuities, characteristic of continental settings. The conglomerates show a coarsening upward sequence and contain clasts of up to 50 cm (diameter) marking high energy depositional settings. The last member is composed of beige-yellow and light green fossiliferous mudstone-sandstone-grainstone alternations. Autochthonous corals and other benthic fossil assemblages are indicative for shallow marine environments.

A preliminary age of the Van Formation, based the earlier documented fossil assemblages (*Miogypsina intermaida, Orbulina suturalis, Globorotalia juanai ect.)*, indicates a Burdigalian - Serravallian age (Demirci, 2016; Sağlam, 2003). These foraminiferal data were derived from the shallow marine member of the formation (VFU + VFL:

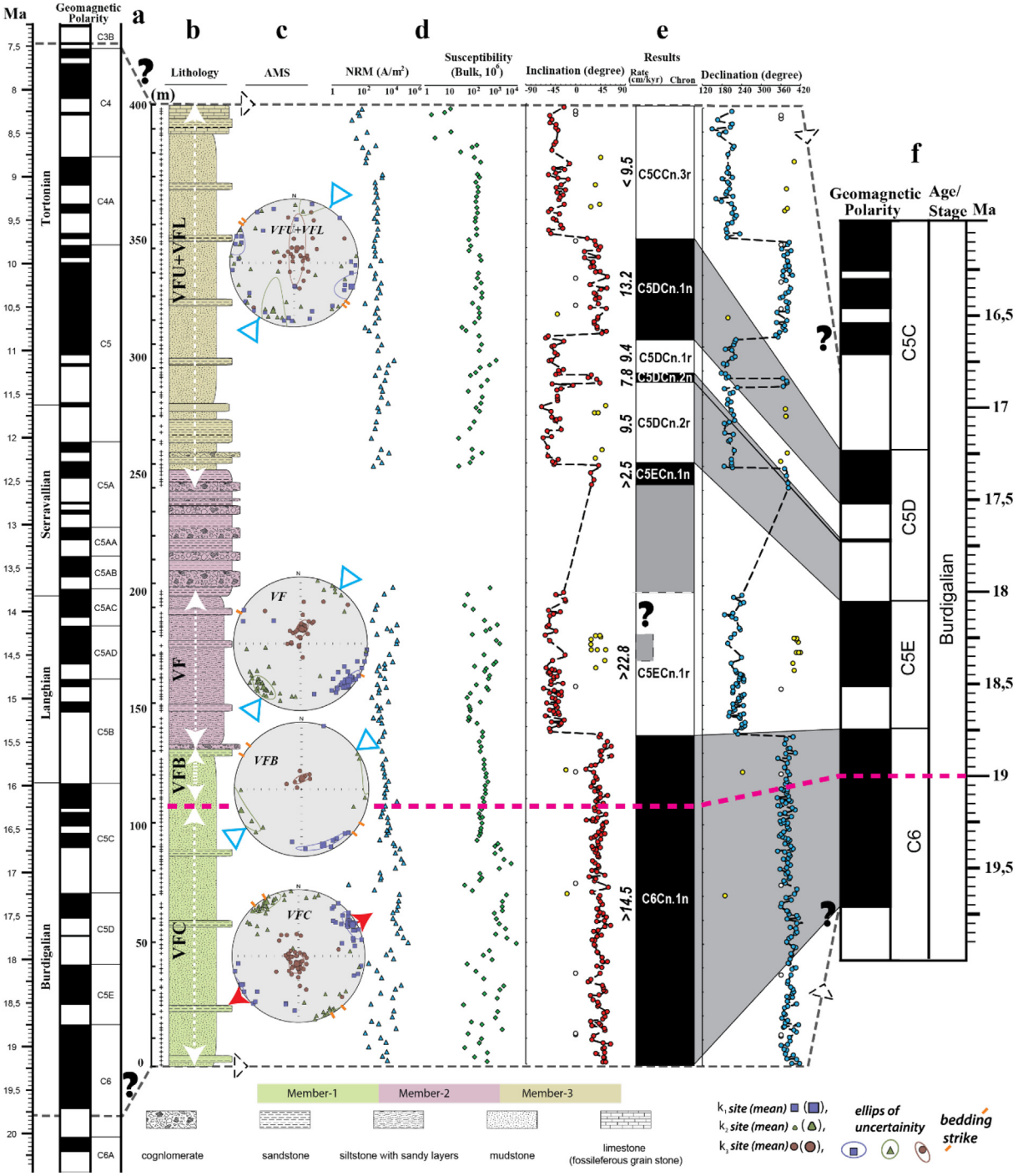

Fig. 2. a) General magnetostratigraphic chart (Hilgen et al., 2012) comprises the early to late Miocene time interval for the study area. b) Measured lithostratigraphic sections (combined) of the sampled Van Formation. c) Equal area plots (lower hemisphere projection) of the three axes of the anisotropy of the magnetic susceptibility ellipsoids from the 4 different lithology units after bedding plane correction. d) Characteristic Remnant Magnetization (ChRM) directions and magnetic susceptibility graphs along the measured stratigraphy. e) Calculated magnetostratigraphic results and correlation with the (f) best fit the reference (Burdigalian) period (Hilgen et al., 2012).

member-3). On the other hand, Acarlar et al. (1991) suggests a late Oligocene – early Miocene age for the base of the formation. This age is also based on fossil assemblages, but potential reworking of Oligocene assemblages cannot be ruled out here.

2.2. The Van Formation in a regional context

The Muş, Elazığ and Malatya basins, located north of the BZSZ, also host Miocene marine sequences. Early Miocene sedimentary rocks in the Muş Basin are represented by shallow marine limestones (Adilcevaz Formation) which have a transitional contact with the underlying Oligocene continental clastics (Ahlat/Kelereş Formation) (Demirtaşlı and Pisoni, 1965; Sancay et al., 2006). The oldest tectonic event here is associated with the commencement of the westward escape of the Anatolian plate (Sengor and Gorür, 1985). West of the Muş basin, the late Oligocene – early Miocene marine Alibonca Formation is exposed in the Elazığ and Malatya basins (Soytürk, 1973; Sönmez, 2004; Türkmen et al., 2011). This formation shows, from bottom to top,

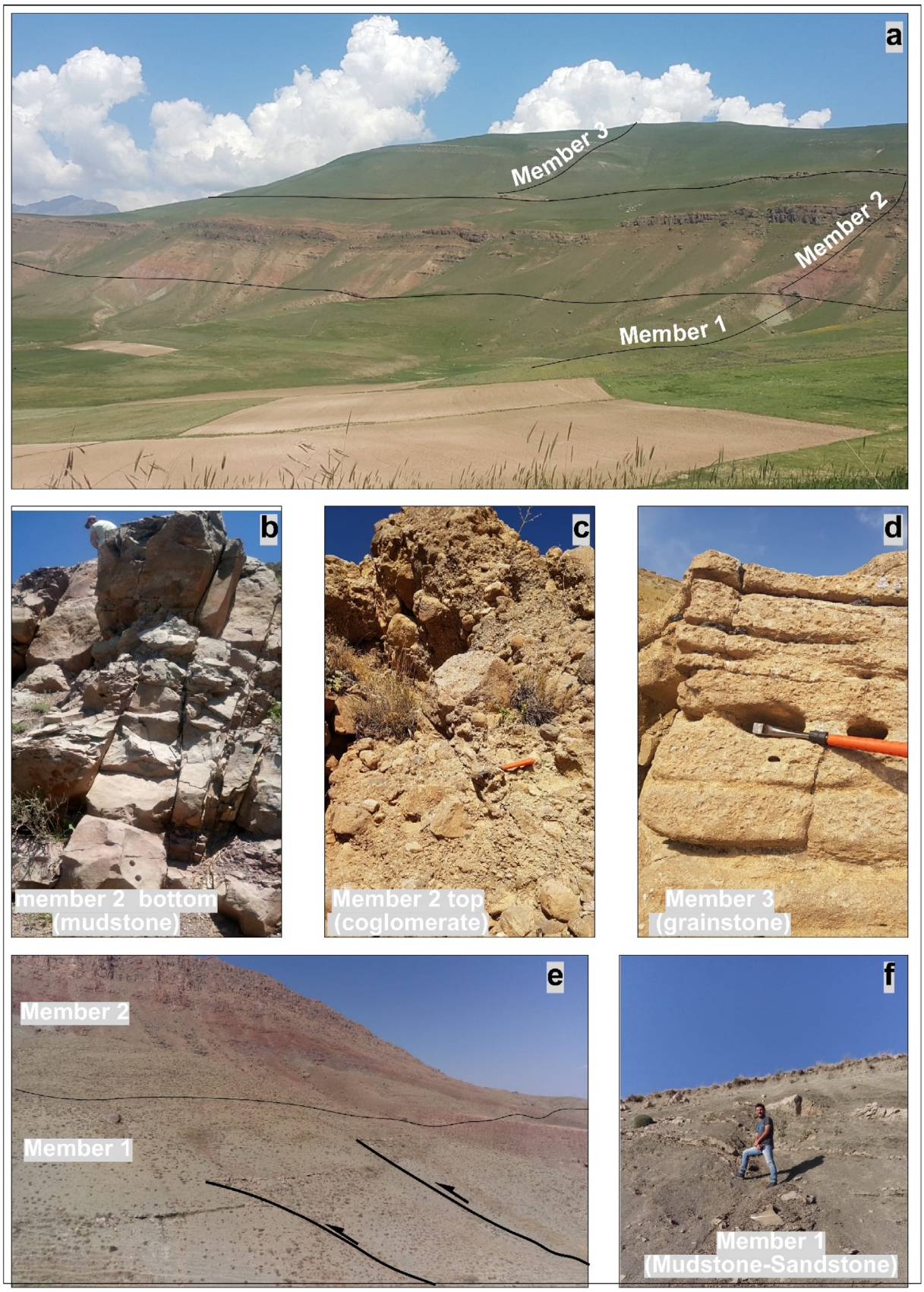

Fig. 3. a) A picture from a distance (2 km) showing the different members of the Van formation. b) Mudstone layers at the base of member 2. c) Conglomerate layers at the top of member 2. d) Grainstone layers of member 3. e) Reverse faults cutting layers of member 1 are sealed by uppermost layers of member 2 where a change in AMS patterns is detected. f) Mudstone-sandstone alternation observed in member 1.

Table 1
a) Anisotropy of magnetic susceptibility (AMS) results from four different sections from the Van Formation, Eastern Anatolia. b) Site mean normal/reverse, and reversed polarity paleomagnetic results from the same locality.

a) Sections	Geog. coord. (deg)		N	Bedding	$k_m \times 10^{-6}$ (SI)	L	F	Pj	T	D/I (k_{max})	D/I (k_{min})	e_1	e_2	e_3
	Lat. (N)	Long. (E)		Azi / dip										
VFB (in situ)	39.50370	32.74693	08	287 / 19	383	1.008	1.049	1.062	0.696	158.8/01.3	258.4/82.3	23.5	24.1	11.6
VFB (tilt corr.)						1.008	1.049	1.062	0.696	158.9/12.0	002.3/77.0	25.9	26.4	11.4
VF (in situ)	39.55369	32.82139	39	287 / 16	416	1.009	1.023	1.034	0.364	129.1/04.0	310.8/86.0	13.9	14.5	12.3
VF (tilt corr.)						1.009	1.023	1.034	0.364	127.2/09.8	005.0/72.0	13.0	14.5	12.3
VFC (in situ)	39.44065	32.93658	43	319 / 15	1510	1.013	1.032	1.048	0.397	060.7/21.1	218.3/68.4	14.1	14.4	12.7
VFC (tilt corr.)						1.013	1.032	1.048	0.397	060.1/06.7	192.6/80.1	14.3	14.5	11.8
VFU + VFL (in situ)	39.61479	32.52476	29	330 / 19	193	1.018	1.031	1.053	0.423	112.2/3.5	011.8/71.2	25.3	46.5	47.2
VFU + VFL (tilt corr.)						1.018	1.031	1.053	0.423	114.6/14.3	308.9/75.2	26.0	46.4	47.3

b)	Lat. (N°)	Long. (E°)	N_m/N_{45}	Dec	ΔD_x	Inc	ΔI_x	k	K	a95	$A95_{min}$	A95	$A95_{max}$
ChRM directions (in situ)													
Normal	39.73907°	32.98141°	201/201	10.5	2.7	53.2	2.4	30.6	19.9	1.8	1.4	2.3	2.9
Reversed			126/123	195.9	3.4	−49.0	3.4	24.4	19.2	2.6	1.8	3.0	4.0
N + R			327/323	12.8	2.1	51.6	2.0	27.5	19.5	1.5	1.2	1.8	2.2
ChRM directions (tilt corrected)													
Normal	39.73907°	32.98141°	201/201	21.0	2.2	41.9	2.7	28.5	25.2	1.9	1.4	2.0	2.9
Reversed			126/124	212.9	3.3	−38.4	4.4	18.7	17.8	3.0	1.7	3.1	3.9
N + R			327/326	25.4	2.0	40.7	2.5	21.8	19.6	1.7	1.2	1.8	2.1

N = number of specimes; km = mean susceptibility; L = magnetic lineation (k_{max}/k_{int}); F = magnetic foliation (k_{int}/k_{min}); Pj = corrected degree of anisotropy $\exp\sqrt{\{2[(n_1\text{-}n)^2 + (n_2\text{-}n)^2 + (n_3\text{-}n)^2\}}$)(Jelinek, 1981); T = shape parameter $(2(n_2\text{-}n_3)/(n_1\text{-}n_3)\text{-}1)$(Jelinek, 1981); e_1, e_2, e_3 = semi-angles of the 95% confidence ellipses araound the principal susceptibility axes (Jelinek, 1981) $n_1 = \ln k_1$, $n_2 = \ln k_2$, $n3 = \ln k_3$,$n = (n_1 + n_2 + n_3)/3$, D (declination) and I(inclination) for k_{max} and k_{min} after tectonic correction. b) N_m/N_{45} number of specimens from which a direction has been interpreted/number of specimens after application of a 45° fixed cut-off on the VGPs, D: declination, I: inclination, ΔD_x: declination error, ΔI_x: inclination error, k: estimate of the precision parameter determined from the ChRM directions, a95: cone of confidence determined from the ChRM directions, K: precision parameter determined from the mean virtual geomagnetic pole (VGP) direction, A95: cone of confidence determined from the mean VGP direction, A95min and A95max correspond to the confidence envelope of Deenen et al. (2011, 2014).

continental red clastics (Çobandere member), shallow marine clastics (Kınık member) and reefal limestones (Suceyin member; Sönmez, 2004). All of the units mentioned above are unconformably overlain by younger volcanics/volcanoclastics and/or continental clastics, and their contacts with underlying Oligocene rocks are transitional. There is no observable connection between these early Miocene marine units in Eastern Anatolia, but stratigraphic studies infer an equival tectono-stratigraphic evolution because of similar ages and tectonic positions. In contrast, the Miocene marine deposits south of the suture zone (e.g. Kahramanmaraş Basin) reveal much younger ages, the youngest documented age being Serravallian (Hüsing et al., 2009).

The termination of marine environments to the north of BZSZ, like in the Van Formation, is generally associated with the uplift/exhumation events on the active Eurasian margin subsequent to continental collision along the BZSZ. In this regard, (i) high resolution dating of the youngest marine unit on the active margin and (ii) understanding responses of possible uplift/exhumation events in sedimentological records are considered crucial to better constrain the timing of continental collision in the region.

3. Methods

3.1. Magnetostratigraphic sampling

Paleomagnetic samples were collected from four different segments of the Van Formation and then combined according to stratigraphic order (Figs. 1d and 2). Standard cylindrical (25 mm Ø) paleomagnetic cores were on average drilled in ~2 m stratigraphic resolution (maximum distance 4 m). We aimed to take at least two samples from each level. In total, 349 samples were collected from the ~400 m-thick Van Formation for magnetostratigraphic and other paleomagnetic analyzes. During sampling, drilling orientations and bedding attitudes were measured using a magnetic compass and then corrected for the present-day declination (International Geomagnetic Reference Field; IGRF) of 4.5°W for the sampling period, June 2017.

3.2. Paleomagnetic analyses

All paleomagnetic and rock magnetic preparations and measurements were carried out at the paleomagnetic laboratory Fort Hoofddijk of Utrecht University, the Netherlands. First, rock magnetic experiments were performed to determine the nature of the magnetic carriers and to develop demagnetization strategies accordingly. In addition, AMS (anisotropy of magnetic susceptibility) measurements were made from 120 suitable (unbroken, whole unit) specimens to retrieve tectonic strain directions. Half of the total 335 specimens were subject to thermal (TH) and the other half to alternating field (AF) stepwise demagnetization to determine natural remnant magnetization (NRM) directions. We intended to perform at least one TH and one AF measurement for each stratigraphic level. The TH demagnetization process was performed by heating in a magnetically shielded oven (ASC, model TD48-SC), which has a residual magnetic field < 10 nT. The demagnetization process started from room temperature (20 °C) up to a maximum temperature of 600 °C (using 20–50 °C steps). After each demagnetization step, the NRM was measured on a 2G Enterprises horizontal cryogenic magnetometer equipped with three DC SQUID (noise level 3×10^{-12} Am^2). The remaining half of the specimens were treated with alternating field demagnetization by means of a laboratory built automated system (Mullender et al., 1993). The demagnetization procedure was carried out with increments of 3–10 mT, up to a maximum of 100 mT. The AF demagnetization and measurement process were performed with an in house built robotized sample handler, attached to a horizontal pass-through 2G Enterprises DC SQUID cryogenic magnetometer (noise level $1–2 \times 10^{-12}$ Am^2) in a magnetically shielded room.

3.3. Rock magnetic analyses

Thermomagnetic experiments were carried out on 15 different samples to determine the nature of the dominant magnetic carrier(s) in different lithologies of the Van Formation. Approximately 50 mg of powdered rock specimen was put into a quartz-glass sample holder and measured in air with heating-cooling rates of 10 °C /minute up to successively higher temperatures (max. 700 °C), using a modified horizontal translation type Curie balance with a sensitivity of $\sim 5 \times 10^{-9}$ Am^2 (Mullender et al., 1993).

The AMS of 120 representative specimens was measured using the Multi-Function Kappabridge MFK1-FA (AGICO-Brno, Czech Republic), equipped with an up-down mechanism and a rotator to determine the magnetic fabric and the potential compaction or tectonic strain. The measurement sensitivity is 10^{-8} SI which is critical for some sedimentary rocks (especially limestones) that exhibit very weak magnetic magnetization properties. The Anisoft 4.2 data browser (Chadima and Jelinek, 2009) was used to illustrate the AMS results and their density distributions. The AMS parameters were calculated according to Jelinek statistics (Jelínek, 1978; Jelínek, 1977) and tilt corrected results are given in Table 1a.

4. Magnetostratigraphic and rock magnetic results

4.1. Rock magnetic and AMS results

Thermomagnetic runs of representative samples from variable lithologies of the Van Formation are shown in Fig. 4a-b. In general, they show various magnetic carriers and a moderately high total magnetization, typically in the range 0.01–0.03 Am^2/kg for the pale colored marls, mud-siltstones and limestones (Fig. 4a). Some gray marls and sandstone dominated lithologies are stronger, and show values above 0.1 Am^2/kg (Fig. 4b).

The thermomagnetic curves of the Van Formation reveal two different magnetic carriers. The irreversible behavior between 200 and 500 °C and the inflection point in magnetization at a temperature of ~350 °C points to the presence of maghemite (Fig. 4a). The major decrease in magnetization at ~580 °C corresponds to the Curie temperature of magnetite (Fig. 4b).

The mean susceptibility (k_m) of 120 specimens is plotted in a histogram and shows a wide range, from values around zero (diamagnetic) to high values of $> 10000 \times 10^{-6}$ SI (ferromagnetic). There are two main clusters, one around 100×10^{-6} and one around 500-5000×10^{-6} SI (Table 1 and Fig. 4c). The k_m values mainly display changes in lithology. In particular, pale-colored calcareous-limestones show low k_m values, while darker mudstones and sandstones provide relatively high k_m values.

Both foliation F(k_2/k_3) and lineation L(k_1/k_2) parameters have small scattering between $1.002 \leq F \leq 1.104$ ($F_{mean} = 1.029$) and $1.001 \leq L \leq 1.074$ ($L_{mean} = 1.011$), respectively. The F_{mean} is slightly higher than the L_{mean} reflecting the mainly oblate character of the distribution (Fig. 4d). The corrected anisotropy degree P_j shows relatively low values ($1.007 \leq P_j \leq 1.162$) with a mean clustering around $P_j = 1.042$ (Table 1 and Fig. 4e).

The equal area (lower-hemisphere) projections of the AMS ellipsoids were grouped in four units according to sampling strategy in the field study. They are VFC, VFB, VF, and VFU + VFL of the sampled the Van Formation, respectively (Fig. 1d and 2c). The oldest part of the formation, the VFC section contains 43 samples and shows well clustering and discrete grouping of the principle susceptibility axes, indicating tectonic deformation other than a sedimentary compaction (k3 is almost perpendicular to the bedding plane). The mean maximum susceptibility orientation (k1), the AMS lineation, was calculated as ~NE-SW (60°N), which is almost perpendicular to the local bedding strike (Fig. 2c, Table 1). The VFB section (8 samples), located just below the marine continental transition, shows a 90° difference in k_1 directions, trending ~NW-SE (158°N). The VF section, total number of 39 measurements, shows moderate to well clustering ($e_{1,2,3} < 50$) of the three principal axes. The mean maximum susceptibility axis (k_1) points to a ~NW-SE (127°N) orientation, similar as in VFB (Fig. 2). The mean minimum susceptibility (k_3) is almost perpendicular to the bedding plane (inclination = 72°), reflecting sedimentary compaction again. The last two sections (VFU and VFL) locate ~2–3 km east of the first group and comprise the upper part of the Van Formation (Fig. 1d). From the top of the thick conglomerate layer, a total of 29 AMS measurements show that distributions of the principal directions are poor to moderately clustered and especially k_1 and k_2 directions are not well differentiated, possibly related to the dominantly calcareous lithologies. Although it has a scattered distribution, the direction of k_3 is still nearly perpendicular to the bedding and the mean maximum anisotropy direction is calculated in NW-SE orientation (~112°N). This orientation is close to the directions calculated in the VFB and VF sections and is also almost parallel to the direction of the local bedding strikes (Table and Fig. 2c).

In order to determine the relationship between magnetic mineral properties and lithology, the bulk susceptibility was compared to the NRM intensities. The susceptibility and NRM graphs show relatively scattered anomalies in the first 100 m of the VFC section, where bulk susceptibility varies between 100-1000 $\times 10^{-6}$(SI) and NRM intensities are clustered around 10,000 μA/m. Between 100 and 150 m in stratigraphic level, roughly corresponding to VFB, the two magnetic properties show less variability with the bulk susceptibility being $\sim 100 \times 10^{-6}$(SI), and the NRM intensities around 8000 μA/m. From the thick conglomerate unit upwards, the upper part (VFU and VFL) of the section again shows more scattering in both values. At the top of the formation (in the last 20 m) both bulk susceptibility and NRM properties significantly decrease to 10×10^{-6}(SI) and 100 μA/m, respectively (Fig. 2d).

4.2. NRM directions and magnetic polarity patterns

We plot the stepwise demagnetization results using Zijderveld vector endpoint diagrams (Zijderveld, 1967). Representative examples for four different stratigraphic levels are shown in Fig. 5a-d. The characteristic remanent magnetization (ChRM) directions were computed by taking at least five to seven or more successive TH or AF steps following the eigenvector approach of (Kirschvink, 1980). In general, magnetic directions (inclinations and declinations) show a linear decrease towards the origin (Fig. 5). In a few specimens, we applied the great-circle approach (McFadden and McElhinny, 1988), especially when the demagnetization diagrams passed by the origin, suggesting multiple components. The normal and reverse polarity and normalized site mean directions were calculated using Fisher (1953) statistics and the distributions were tested according to the criteria of Deenen et al. (2011). We applied a fixed 45° cut-off on the corresponding VGP distributions, while errors in declinations (ΔDx) and inclinations (ΔIx) were calculated from A95 (the 95% cone of confidence of VGPs) following (Butler, 1992). All interpretations and statistical procedures were completed using the on-line portal of Paleomagnetism.org (Koymans et al., 2016).

The NRM results were grouped into high and low quality or no demagnetization results based on the characteristics of the Zijderveld vector endpoint diagrams (Zijderveld, 1967). High quality data are those with consistent NRM directions by both demagnetization methods (TH / AF), and using at least 5 successive points on a progressive decay towards the origin. In addition, these samples allow interpretation of AF/TH demagnetization steps up to 50 mT and 450 °C. The high-quality inclination and declination values from the TH and AF demagnetization results are displayed as red and blue colored spheres in Fig. 2. Low quality data are those diagrams that do not pass the above criteria, but do show a linear progress (not necessarily towards the origin). More specifically, these comprise NRM directions from low demagnetization

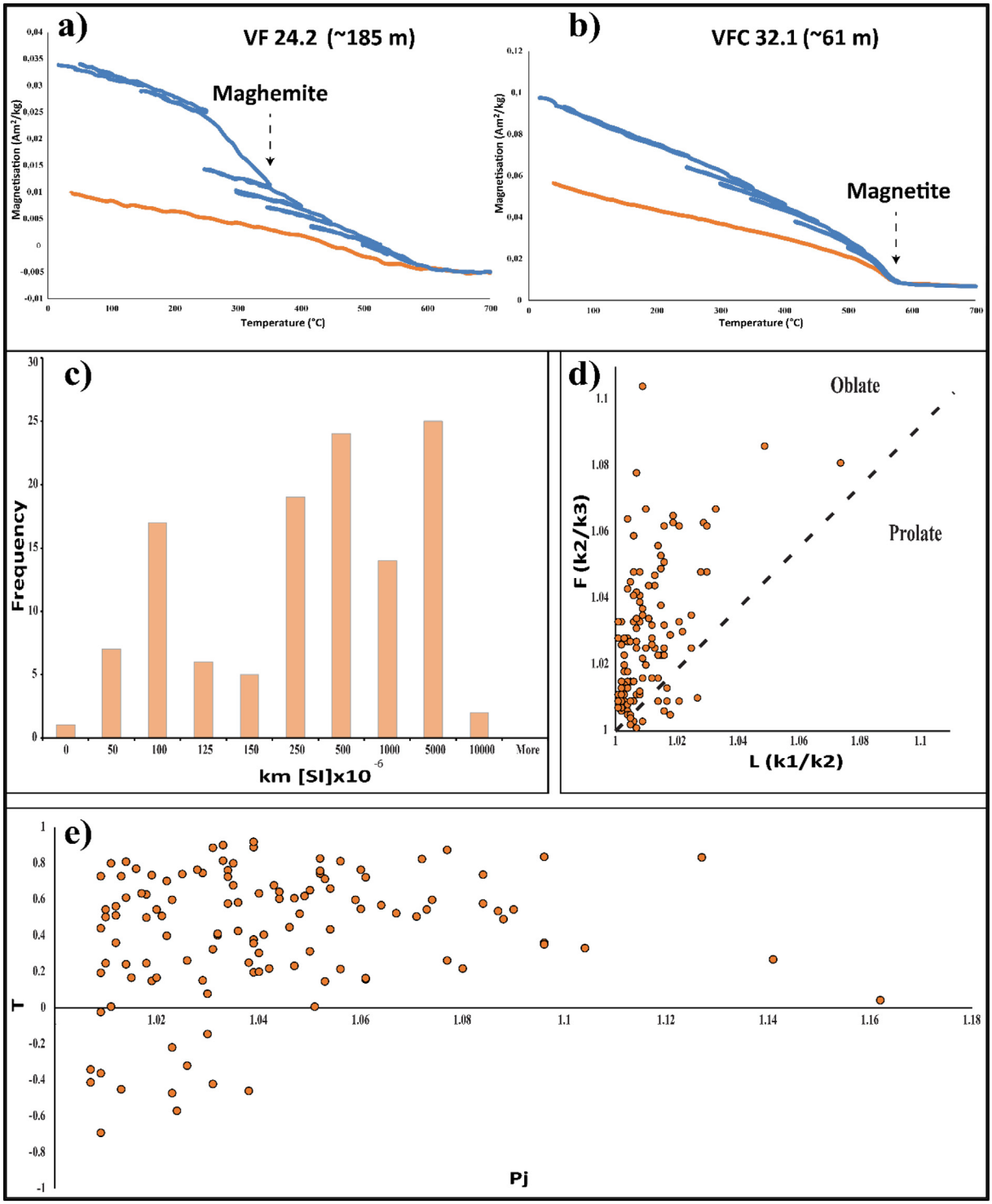

Fig. 4. a-b) Curie-Balance results of two representative samples of the Van Formation. Thermomagnetic curves consist of a number of heating-cooling cycles to monitor changes (alterations) in magnetic mineralogy (Mullender et al., 1993). The final cooling curves are indicated with the orange lines. See the text for explanation of the thermomagnetic behavior. c) Statistical distribution of the susceptibility (km) values. d) Flinn diagram of foliation (F = k2/k3) and lineation (L = k1/k2). AMS values for individual specimens of all measurements. Measured ellipsoids show dominantly oblate in shape. e) Plot of shape factor (T) versus corrected anisotropy degree (Pj).

steps (< 300 °C and 25 mT in TH and AF, respectively), directions represented by < 5 consecutive steps, and directions with conspicuous or inconclusive declination and inclination values.

In addition, a few scattered normal polarity NRM directions were obtained at stratigraphic levels within a dominantly reversed interval (Fig. 2). These results are incompatible with the general trend and are interpreted to represent a present-day field overprint component. Finally, some diagrams showed too weak magnetization to determine a representative magnetic direction. The low quality, and the “no results”, samples are marked in yellow and white colour, respectively (Fig. 2e).

Plotted in stratigraphic order, the magnetostratigraphic results of

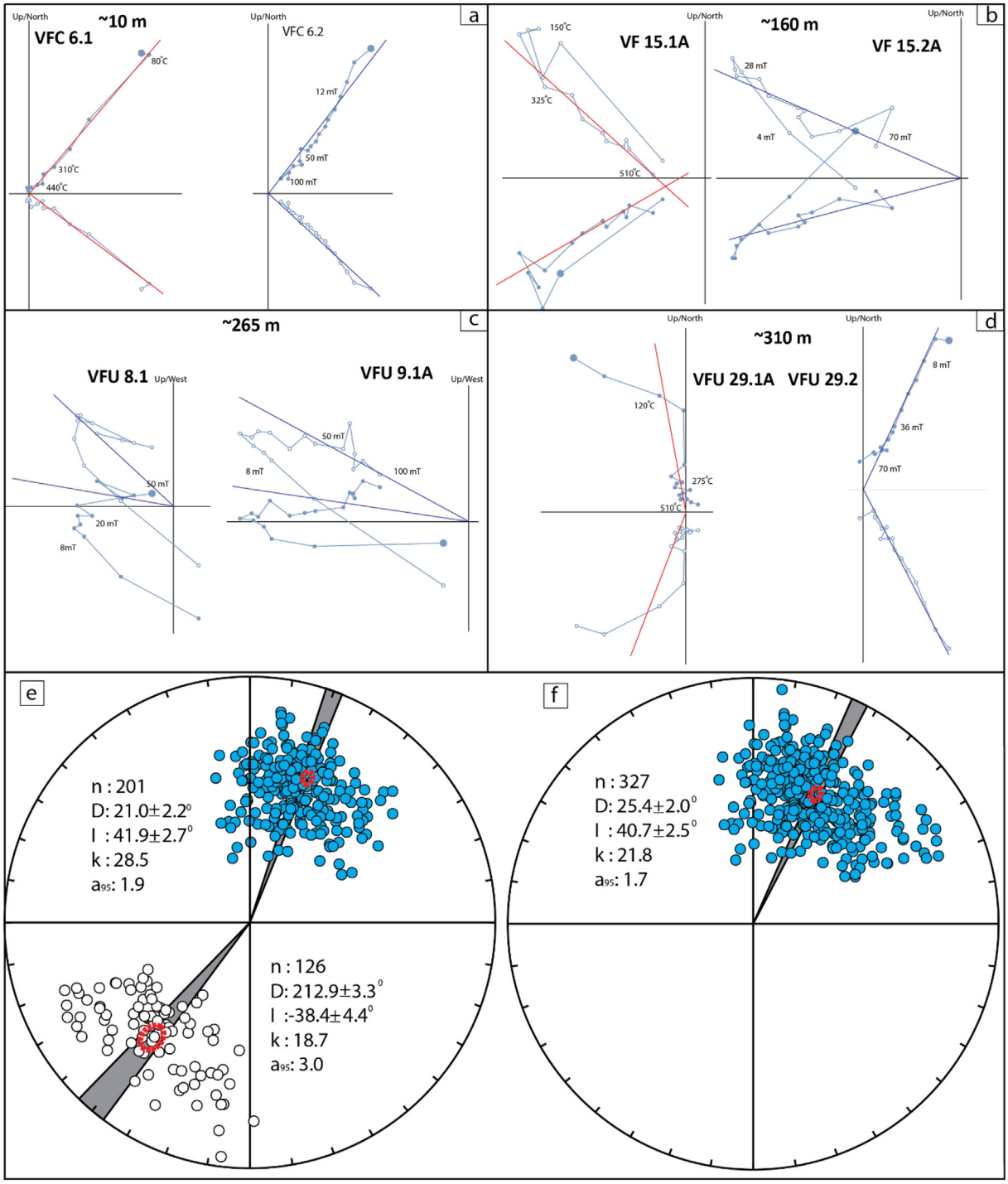

Fig. 5. a-d) Zijderveld representation of the NRM results from four different stratigraphic levels and two different demagnetization protocols represented by red (TH) and blue (AF) lines, respectively. e) Equal area projection of both normal and reversed ChRM directions after tilt correction (TC) and, f) normalized magnetization results. (For interpretation of the references to colour in this figure legend, the reader is referred to the web version of this article.)

the Van Formation show four normal and four reversed polarity intervals. Some intervals (e.g. 175–185 m) show various samples which only contain a present-day field overprint (Fig. 2e). In addition, the interval between 195 and 240 m could not be sampled due to the limited number of outcrops and the presence of thick conglomeratic layers. The results of these two parts are shown as gray colors in the magnetostratigraphic polarity interpretation column (Fig. 2e).

The mean ChRM directions from the total amount of 330 high quality demagnetization diagrams indicate that both normal and reversed polarity mean directions show significant amount of clockwise rotation in tectonic coordinates (D/I: 21.0 ± 2.2° / 41.9 ± 2.7° and D/I: 212.9 ± 3.3° / -38.4 ± 4.4°, respectively) (Fig. 5e, f). A rotation difference of about 10° was calculated between the mean normal and reversed polarity directions. This discrepancy may be explained by an incompletely removed overprint with partially overlapping unblocking spectra. These normal polarity overprints are probably related to a Viscous Remanent Magnetization (VRM) of the Brunhes chron, which is especially recognizable in the reversed polarity samples (Fig. 5b and c).

The normal polarity ChRM distributions, in situ and tilt corrected, show a statistically similar scatter before (K = 19.9, A95 = 2.3) and

after tilt correction (K = 25.2, A95 = 2.0). The reversed polarity ChRM distributions show slightly higher scatter both in situ and tilt corrected (K = 19.2, A95 = 3.0 and K = 17.8, A95 = 3.1) (Table 1b). The combined statistical results, after normalizing the reversed polarities, show an average declination of 25.4 ± 2.0°. We thus conclude that a significant clockwise rotation of the region must have taken place after deposition of the sediments (Fig. 5f).

5. Discussion

5.1. Magnetostratigraphic dating and sediment accumulation rates (Van Formation)

The Van Formation comprises four normal and four reversed magnetic polarity intervals (Fig. 2). In order to determine the magnetostratigraphic age and the derived sedimentation rates, we compared the observed paleomagnetic polarity pattern with the Global Polarity Time Scale (Hilgen et al., 2012). The optimal correlation of the section is obtained by correlating the lowermost long normal polarity interval to chron C6Cn.1n and the uppermost long normal polarity interval to C5DCn.1n (Fig. 2f). The characteristic small third normal polarity interval then correlates to C5DCn.2n. These chrons roughly correspond to the lower-middle Burdigalian and suggest that the section straddles the time interval between ~19.7 to ~16.75 Ma. (Fig. 2). The transition from deep marine marls (VFC + VFB) to continental clastics (VF) occurs at the top of C6Cn.1n at an age of 18.75 Ma. Terrestrial conditions prevailed until 18 Ma (upper part of C5ECn.1n) in the Van region, after which shallow marine conditions (VFU + VFL) were installed, lasting at least until 17 Ma (Fig. 2).

This correlation allows us to calculate the sediment accumulation rates throughout the section. The 140 m thick deep marine succession of VFC and VFB shows an average sediment accumulation rate of 0.145 m/Myr. The 110 m-thick VF section of mainly red continental clastics has been deposited at > 0.228 m/Myr, while the ~50 m-thick non-sampled conglomerate-sandstone layers at its top comprise a time interval of ~300 kyr. The sharp increase in sediment accumulation rate at the marine-continental transition is probably attributed to the rapid energy increase in depositional setting after the demise of deep marine-dominated sequences. The shallow marine grainstone-mudstone alteration of the VFU and VFL sections show sediment accumulation rates between 0.025 and 0.132 m/Myr. The lowest rates at the bottom and top parts of the section are related to deposition of grainstones/limestones. The decrease in sediment accumulation rate in the upper unit is considered the result of a stagnation period possibly related to the low-energy stabilization subsequent to rapid uplift/erosion events in the region. In summary, we conclude that the observed fluctuations in sediment accumulation rate throughout the section are consistent with the sedimentological characteristics of the members.

5.2. Tectonic deformation and AMS relations

The AMS results calculated from four different sections indicate a change from low to moderate level of tectono-magnetic fabrics in the Van Formation. The tectono-magnetic fabrics are evidenced by well-defined foliations (k3) coinciding with bedding poles and distinct magnetic lineations (k1 and k2) of low error ellipsoids (Table 1a and Fig. 2c). These AMS patterns can assert the style of deformation by associating it with local or regional kinematic observations (bedding, fault, fold, etc.) (e.g., Mattei et al., 1997; Scheepers and Langereis, 1994; Soto et al., 2009). In general, weak to medium contractional deformation shows magnetic anisotropy lineation (k_1) (the most elongated axes of strain ellipsoid) perpendicular to the shortening direction. (e.g. Borradaile and Henry, 1997; Housen et al., 1996; Kissel et al., 1997; Mattei et al., 1997; Özkaptan and Gülyüz, 2019; Pares et al., 1999; Sagnotti et al., 1994; Soto et al., 2009). In this case, k_1 is generally parallel to the fold axis/bedding strike and the k3 axis becomes parallel to shortening direction. On the other hand, extensional deformation makes the k_1 axis aligned perpendicularly to the bedding strike or main normal faults (e.g. Cifelli et al., 2005; Mattei et al., 1997).

Based on these definitions; our AMS results indicate two different deformation patterns within the Van Formation (Fig. 2). The older pattern is observed in the VFC section (member-1) and is represented by extension-related deformation ellipsoids, as the mean k_1 direction is perpendicular to the bedding strike here. The younger parts of the section (member-2&3) are associated with a contractional regime; k_1 being parallel to the bedding strike. The younger parts, especially VFU + VFL, show slightly higher scatter in K1 and K2 which may indicate a sedimentary to slight tectonic deformation (contraction) in the final phase. Apparently, the younger compressional deformation was not intense enough to deform the earlier magneto-fabrics that shaped under extensional stress. We thus conclude that a major change from extensional to compressional deformation is dated at 19 Ma, closely before the marine continental transition.

5.3. General implications

Subduction and obliteration of the southern Neo-Tethys Ocean are the main tectonic processes that influence the Neogene geology of Eastern Anatolia. The progressive demise of the ocean between the Eurasian and Arabian plates gave way to the development of the Bitlis-Zagros Suture Zone (BZSZ) during the Neogene (Şengör et al., 2003; Şengör and Yılmaz, 1981). The Arabian plate was a passive margin with a promontory oceanic slab on its northern extension during the subduction period while the Eurasian plate formed an active margin in the north. This paleogeographic configuration caused deposition of foreland basin deposits between the Eurasian and Arabian margins (e.g., Hüsing et al., 2009). In addition to these, marine sequences accumulated on the Eurasian plate (at the north of BZSZ) in the Elazığ, Muş, Malatya and Van basins (Aktaş and Robertson, 1984; Hüsing et al., 2009; Kaymakcı et al., 2006). This implies a genetic link between the foreland region and the active margin. This association was previously explained by two possible scenarios; i) back-arc extension or ii) development of a retro-arc foreland basin array at the north of suture zone (Hüsing et al., 2009; Darin et al., 2018). However, another putative scenario exists for the active Eurasian margin. This scenario is explained by the development of an extensional fore-arc basin at the southernmost tip of the Eurasian margin (Fig. 6a&b). Our AMS directions, indicating extension up to 19 Ma and contraction afterwards, in principle support both the back-arc extension & extensional fore-arc scenario (Fig. 6). We consider, however, extension in the fore-arc region more suitable for the Van region, because of the presence of ~20 Ma old arc-related magmatic rocks north of the accreted Bitlis massif (Açlan and Altun, 2018; Açlan and Duruk, 2018; Oyan, 2018). In such a setting, subsequent collision might have resulted in contractional tectonics and related uplift events in the fore-arc region. This caused a switch in depositional environments from extensional fore-arc to compressional piggy-back basin setting, while deposition continued in the main foreland region (Fig. 6c). A rapid increase in sediment accumulation rates during the compressional stage also supports piggy-back basin evolution. This rapid increase may be associated with enhanced subsidence related to the load of the propagating landmass, and the proximal sediment source position (c.f. Zoetemeijer et al., 1993; DeCelles and Giles, 1996). Although there is only limited literature on accumulation rates in piggy-back or foreland basins, several magnetostratigraphy-based studies have revealed similar accumulation rate trends as the results presented in this study (e.g Ohja et al., 2009; Beamud et al., 2011; Li et al., 2011).

Hüsing et al. (2009) and Koshnaw et al. (2019) suggest ages of 11 Ma and 26 Ma for the timing of Eurasia-Arabia continental collision, respectively. The first age is based on the age of the youngest marine unit found below subduction-related thrust faults in the

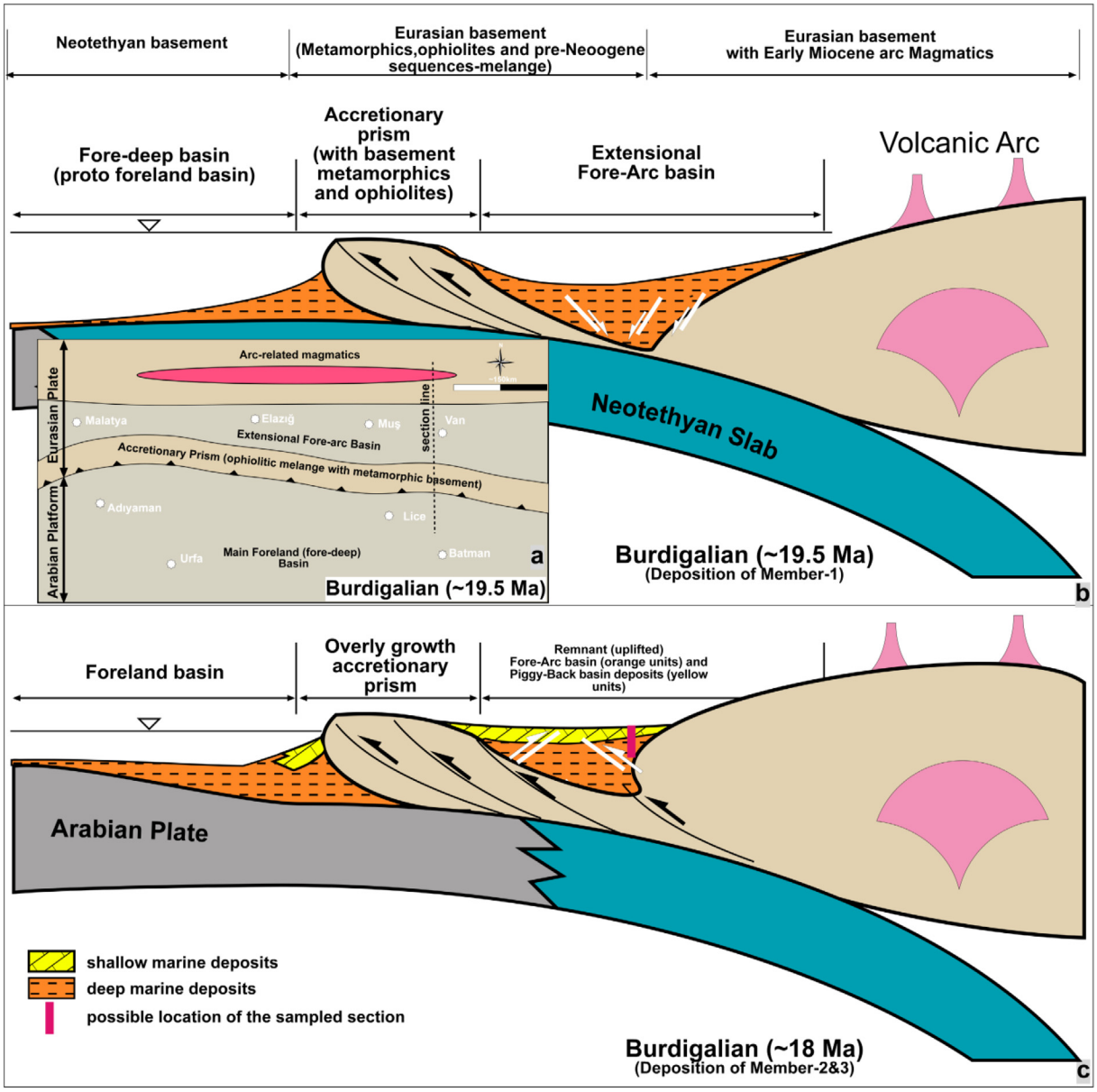

Fig. 6. New tectono-stratigraphic model for the sedimentary successions deposited in the foreland and fore-arc regions in front of the Bitlis-Zagros Suture Zone and on the Eurasian margin during the early Miocene. a) Schematic palinspastic map of Eastern Anatolia for ~19.5 Ma. b) Tentative model showing the extensional phase related to the configuration of the Eastern Anatolian active margin at 19.5 Myr ago and depositional setting of the deep marine member in extensional fore-arc settings, location of the cross-section is marked as a dotted line in "a". c) Tentative model showing the contractional phase-related configuration of the Eastern Anatolian active margin at ~18 My ago and the depositional setting of the continental and shallow marine member. Note 1: The AMS results of our study also suggest extensional settings up to 19 Ma and contractional settings after 19 Ma for the Eurasian active margins. Note 2: Arc-related magmatic rocks in "a" are attributed to magmatic rocks dated in Açlan and Duruk (2018), Açlan and Altun (2018) and Oyan (2018).

Kahramanmaraş Basin. This region is, however, still being exposed to N-S contraction and therefore we consider the classification of the thrust faults as subduction-related or post-collisional convergence-related as questionable. The low-temperature thermo-chronology database in Darin et al. (2018) presents exhumation ages of ~50 to ~15 Ma (fission track and apatite-helium ages) for the Cenozoic clastics of the Sivas basin and ages of 45–40 Ma and 20 Ma for the soft and hard Eurasia-Arabia collision, respectively. They also suggest that a contractional regime existed since the Paleocene in Eastern Anatolia. However, collision associated exhumation ages of the Sivas basin, located ~350 km north of the BZSZ, suggest that a long lasting contractional regime as driving force for the Eocene and early Miocene exhumation events might be an over interpretation related to the far away position of the Sivas basin. On the other hand, the exhumation ages of the Sivas Basin can potentially be related to extensional tectonics in the back arc region. Also, Koshnaw et al. (2019) do not give a robust (accurate) time constraint because they base their age on the youngest population age of zircon grains collected from a red bed sequence in the Arabian foreland. This population age must be older than the collision due to the additional travel histories of the zircon grains. Zhang et al. (2017) presents zircon ages of Paleocene to lower Pliocene clastics of SW Iran (Zagros belt), but in contrast to Koshaw et al. (2019), they suggest an 11–5 Ma time interval for the collision event along the southwestern portion of the suture zone. The formation ages of magmatic rocks, representing collisional or post-collisional geochemistry, and exhumation ages of crystalline rocks in Eastern Anatolia both vary between ~30 Ma to recent. To sum up, there is at present no clear time constraint for the Arabia-Eurasia collision event that occurred in

Eastern Anatolia along the BZSZ.

We date the onset of contractional settings that may represent the beginning of continental (hard) collision along the BZSZ at ~19 Ma, based on magnetostratigraphically dated AMS results and clear changes in depositional setting. The rapid increase in sedimentation rate in the continental deposits of the Van Formation further supports the idea that the marine-continental transition in the region corresponds to the start of continental collision – related rapid uplift events in the fore-arc region. The decrease in sedimentation rate along the last member (fossiliferous grainstones) of the formation can be attributed to the energy stabilization in the depositional setting after the hard-continental collision and gentle closure of Neo-Tethyan gateway between Mediterranean Sea and Indian Ocean on the Eurasian Plate.

6. Conclusions

The Van Formation represents the youngest marine unit on the Eurasian Plate in SE Anatolia. It is subdivided into three members, represented by 1) deep marine, 2) continental and 3) shallow marine deposits. Paleomagnetic analyses, including thermal and alternating field demagnetization and AMS measurements, revealed primary magnetic components in the Van Formation of Eastern Anatolia. Our resulting magnetostratigraphic data indicate that:

1) The depositional age of the entire Van Formation covers the ~19.75 to ~16.75-time interval, which corresponds to the Burdigalian.
2) The deep marine marls of lower part of the section (VFC, VFB) were deposited in the time interval 19.5–18.75 Ma, in an overall extensional setting.
3) A marine-continental transition took place at an age of 18.75 Ma, coinciding with a conspicuous change from extensional to contractional AMS patterns.
4) The reddish continental part of the section (VF) was deposited between 18.75 and 18 Ma, with an increased sediment accumulation rate.
5) The shallow marine grainstones of the upper part of the section (VFU, VFL) are dated between 18 and 16.75 Ma and mark the final phase of the marine southern Neo-Tethys corridor.

The commencement of continental high energy deposition and contractional regimes (based on AMS results) is dated at ~19 Ma. This age marks the onset of continental (hard) collision along the BZSZ and the initiation of collision related uplift in the region. Our results indicate that an extensional fore-arc basin developed in the Van region at the southernmost tip of the Eurasian margin. Subsequent collision resulted in contractional tectonics and uplift of the fore-arc region. This caused a switch in depositional environments from extensional fore-arc to compressional piggy-back basin setting, possibly associated with enhanced subsidence related to the load of the propagating Arabian landmass.

Declaration of Competing Interest

The authors declare that they have no known competing financial interests or personal relationships that could have appeared to influence the work reported in this paper.

Acknowledgements

This study was supported by the Scientific and Technical Research Council of Turkey (TÜBİTAK, ÇAYDAG-117Y287) for field work and measurements at the Utrecht University, the Netherlands. The study benefited from discussions with Nuretdin Kaymakcı and Cor Langereis. We would like to thank Çetin Yeşilova, Nilay Gülyüz and Fatih Karaoğlan for their valuable comments on the earlier version of the manuscript. We furthermore acknowledge the constructive comments of Daniel Pastor-Galan and an anonymous reviewer.

Appendix A. Supplementary data

Supplementary data to this article can be found online at https://doi.org/10.1016/j.gloplacha.2019.103089.

References

Acarlar, M., Bilgin, A.Z., Elibol, E., Erkan, T., Gedik, İ., Güner, E., Hakyemez, Y., Şen, A.M., Uğuz, M.F., Umut, M., 1991. "Van Gölü Doğu ve Kuzeyinin Jeolojisi", MTA Raporu, No:9469. Ankara.

Açlan, M., Altun, Y., 2018. Syn-collisional I-type Esenköy Pluton (Eastern Anatolia-Turkey): an indication for collision between Arabian and Eurasian plates. J. Afr. Earth Sci. 142, 1–11. https://doi.org/10.1016/J.JAFREARSCI.2018.02.019.

Açlan, M., Duruk, H.İ., 2018. Geochemistry, zircon U-Pb geochronology, and tectonic setting of the Taşlıçay Granitoids, Eastern Anatolia, Turkey. Arab. J. Geosci. https://doi.org/10.1007/s12517-018-3674-4.

Aktaş, G., Robertson, A.H.F., 1984. The Maden complex, SE Turkey: evolution of a Neotethyan active margin. Geol. Soc. London 17, 375–402 Spec. Publ.

Allen, M.B., Armstrong, H.A., 2008. Arabia-Eurasia collision and the forcing of mid-Cenozoic global cooling. Palaeogeogr. Palaeoclimatol. Palaeoecol. https://doi.org/10.1016/j.palaeo.2008.04.021.

Beamud, E., Muñoz, J.A., Fitzgerald, P.G., Baldwin, S.L., Garces, M., Cabrera, L., Metcalf, J.R., 2011. Magnetostratigraphy and detrital apatite-fission track thermochronology in syntectonic conglomerates constraints on the exhumation of the South-Central Pyrenees. Basin Res. 23, 309–331.

Borradaile, G.J., Henry, B., 1997. Tectonic applications of magnetic susceptibility and its anisotropy. Earth-Sci. Rev. 42, 49–93. https://doi.org/10.1016/S0012-8252(96)00044-X.

Butler, R.F., 1992. Paleomagnetism: Magnetic Domains to Geologic Terranes. Blackwell Scientific Publications, Boston.

Cavazza, W., Cattò, S., Zattin, M., Okay, A.I., Reiners, P., 2018. Thermochronology of the Miocene Arabia-Eurasia collision zone of southeastern Turkey. Geosphere. https://doi.org/10.1130/GES01637.1.

Chadima, M., Jelinek, V., 2009. Anisoft 4.2: Anisotropy Data Browser For Windows. Agico. Inc, Brno.

Cifelli, F., Mattei, M., Chadima, M., Hirt, A.M., Hansen, A., 2005. The origin of tectonic lineation in extensional basins: combined neutron texture and magnetic analyses on 'undeformed' clays. Earth Planet. Sci. Lett. 235, 62–78.

Darin, M.H., Umhoefer, P.J., Thomson, S.N., 2018. Rapid late Eocene exhumation of the Sivas Basin (Central Anatolia) driven by initial Arabia-Eurasia collision. Tectonics 37, 3805–3833. https://doi.org/10.1029/2017TC004954.

DeCelles, P.G., Giles, K.A., 1996. Foreland basin systems. Basin Res. 8, 105–123.

Deenen, M.H., Van Hinsbergen, D.J.J., Langereis, C.G., 2011. New reliability criteria for paleomagnetic data sets: an alternative statistical approach in paleomagnetism. Geophys. J. Int. 186, 509–520.

Demirci, E., 2016. Akın ve Taşkonak Köyleri Dolaylarında Yüzeyleyen Serravaliyen-Tortoniyen (Orta-Geç Miyosen) Yaşlı Van Formasyonu Çökellerinin Mikrofasiyes ve Mikropaleontoloji Özellikleri. Yüzüncü Yıl Universitesi.

Demirtaşlı, E., Pisoni, C., 1965. The geology of Ahlat-Adilcevaz area (North of Lake Van). Bulletin of the Mineral Research and Exploration Institute of Turkey 64, 24–39.

Ercan, T., Fujitani, T., Matsuda, J.I., Tokel, S., Notsu, K., Ul, T., Can, B., Selvi, Y., Yıldırım, T., Fisekçi, A., 1990. The origin and evolution of the Cenozoic volcanism of Hasandagı–Karacadag area, Central Anatolia. Jeomorfol. Derg. 18.

Fisher, R.A., 1953. Dispersion on a sphere. Proc. R. Soc. Lond. A217, 295–305.

Hilgen, F.J., Lourens, L.J., Van Dam, J.A., Beu, A.G., Boyes, A.F., Cooper, R.A., Krijgsman, W., Ogg, J.G., Piller, W.E., Wilson, D.S., 2012. The Neogene Period. In: The Geologic Time Scale. Elsevier. https://doi.org/10.1016/B978-0-444-59425-9.00029-9. 2012.

Housen, B.A., Tobin, H.J., Labaume, P., Leitch, E.C., Maltman, A.J., Shipley, T., Ogawa, Y., Ashi, J., Blum, P., Bruckmann, W., Felice, F., Fisher, A., Goldberg, D., Henry, P., Jurado, M.J., Kastner, M., Laier, T., Meyer, A., Moore, J.C., Moore, G., Peacock, S., Rabaute, A., Steiger, T., Underwood, M., Xu, Y., Yin, H., Zheng, Y., Zwart, G., 1996. Strain decoupling across the decollement of the Barbados accretionary prism. Geology 24, 127–130. https://doi.org/10.1130/0091-7613(1996)024<0127:SDATDO>2.3.CO.

Hüsing, S.K., Zachariasse, W.J., van Hinsbergen, D.J.J., Krijgsman, W., Inceöz, M., Harzhauser, M., Mandic, O., Kroh, A., 2009. Oligo-Miocene foreland basin evolution in SE Anatolia: constraints on the closure of the eastern Tethys gateway. In: van Hinsbergen, D.J.J., Edwards, M.A., Govers, R. (Eds.), Geodynamics of Collision.

Jelínek, V., 1977. The Statistical Theory of Measuring Anisotropy of Magnetic Susceptibility of Rocks and Its Application. Geofyzika.

Jelínek, V., 1978. Statistical processing of magnetic susceptibility measured on groups of specimens. Stud. Geophys. Geod. 22, 50–62.

Karaoğlan, F., Parlak, O., Hejl, E., Neubauer, F., Klötzli, U., 2016. The temporal evolution of the active margin along the Southeast Anatolian Orogenic Belt (SE Turkey): evidence from U–Pb, Ar–Ar and fission track chronology. Gondwana Res. 33, 190–208. https://doi.org/10.1016/J.GR.2015.12.011.

Kaymakcı, N., İnceöez, M., Ertepınar, P., 2006. 3D-architecture and Neogene evolution of the Malatya Basin: inferences for the kinematics of the Malatya and Ovacık fault zones. Turkish. J. Earth Sci. 15, 123–154.

Keskin, M., 2003. Magma generation by slab steepening and breakoff beneath a subduction-accretion complex: an alternative model for collision-related volcanism in

Eastern Anatolia, Turkey. Geophys. Res. Lett. 30, 8046. https://doi.org/10.1029/2003GL018019.
Keskin, M., Pearce, J.A., Mitchell, J.G., 1998. Volcano-stratigraphy and geochemistry of collision-related volcanism on the Erzurum-Kars Plateau, northeastern Turkey. J. Volcanol. Geotherm. Res. https://doi.org/10.1016/S0377-0273(98)00063-8.
Kirschvink, J.L., 1980. The least-squares line and plane and the analysis of palaeomagnetic data. Geophys. J. R. Astrol. Soc. 62, 699–718.
Kissel, C., Laj, C., Lehman, B., Labyrie, L., Bout-Roumazeilles, V., 1997. Changes in the strength of the Iceland–Scotland overflow water in the last 200,000 years: evidence from magnetic anisotropy analysis of core SU90–33. Earth Planet. Sci. Lett. 152, 25–36. https://doi.org/10.1016/S0012-821X(97)00146-5.
Koçyiğit, A., 2013. New field and seismic data about the intraplate strike-slip deformation in Van region, East Anatolian plateau. E. Turkey. J. Asian Earth Sci. https://doi.org/10.1016/j.jseaes.2012.11.008.
Koçyiğit, A., Yilmaz, A., Adamia, S., Kuloshvili, S., 2001. Neotectonics of east anatolian plateau (turkey) and lesser caucasus: Implication for transition from thrusting to strike-slip faulting. Geodin. Acta. https://doi.org/10.1080/09853111.2001.11432443.
Koshnaw, R.I., Stockli, D.F., Schlunegger, F., 2019. Timing of the Arabia-Eurasia continental collision-Evidence from detrital zircon U−Pb geochronology of the Red Bed Series strata of the northwest Zagros hinterland, Kurdistan region of Iraq. Geology. https://doi.org/10.1130/G45499.1.
Koymans, M.R., Langereis, C.G., Pastor-Galán, D., van Hinsbergen, D.J.J., 2016. Paleomagnetism.org: an online multi-platform open source environment for paleomagnetic data analysis. Comput. Geosci. 93, 127–137. https://doi.org/10.1016/j.cageo.2016.05.007.
Li, C., Dupont-Nivet, G., Guo, Z., 2011. Magnetostratigraphy of the Northern Tian Shan foreland, taxi he section, China. Basin Res. 23, 101–117.
Mattei, M., Sagnotti, L., Faccenna, C., Funiciello, R., 1997. Magnetic fabric of weakly deformed clay-rich sediments in the Italian peninsula: Relationship with compressional and extensional tectonics. Tectonophysics 271, 107–122. https://doi.org/10.1016/S0040-1951(96)00244-2.
McFadden, P.L., McElhinny, M.W., 1988. The combined analysis of remagnetisation circles and direct observations in paleomagnetism. Earth Planet. Sci. Lett. 87, 161–172.
McQuarrie, N., Van Hinsbergen, D.J.J., 2013. Retrodeforming the Arabia-Eurasia collision zone: age of collision versus magnitude of continental subduction. Geology. https://doi.org/10.1130/G33591.1.
Mullender, T.A.T., Van Velzen, A.J., Dekkers, M.J., 1993. Continuous drift correction and separate identification of ferrimagnetic and paramagnetic contribution in thermomagnetic runs. Geophys. J. Internat. 114, 663–672.
Ohja, T.P., Butler, R.F., DeCelles, P.G., Quade, J., 2009. Magnetic polarity stratigraphy of the Neogene foreland basin deposits of Nepal. Basin Res. 21, 61–90.
Okay, A.I., Zattin, M., Cavazza, W., 2010. Apatite fission-track data for the Miocene Arabia-Eurasia collision. Geology. https://doi.org/10.1130/G30234.1.
Oyan, V., 2018. Ar−Ar dating and petrogenesis of the Early Miocene Taşkapı-Mecitli (Erciş-Van) granitoid, Eastern Anatolia Collisional Zone, Turkey. J. Asian Earth Sci. https://doi.org/10.1016/j.jseaes.2018.03.002.
Oyan, V., Keskin, M., Lebedev, V.A., Chugaev, A.V., Sharkov, E.V., 2016. Magmatic evolution of the Early Pliocene Etrüsk stratovolcano, Eastern Anatolian Collision Zone, Turkey. Lithos. https://doi.org/10.1016/j.lithos.2016.03.017.
Özdemir, Y., Güleç, N., 2014. Geological and geochemical evolution of the quaternary süphan stratovolcano, Eastern Anatolia, Turkey: evidence for the lithosphere-asthenosphere interaction in post-collisionalvolcanism. J. Petrol. https://doi.org/10.1093/petrology/egt060.
Özdemir, Y., Mercan, Ç., Oyan, V., Özdemir, A.A., 2019. Composition, pressure, and temperature of the mantle source region of quaternary nepheline-basanitic lavas in Bitlis Massif, Eastern Anatolia, Turkey: a consequences of melts from Arabian lithospheric mantle. Lithos. 328–329, 115–129. https://doi.org/10.1016/j.lithos.2019.01.020.
Özkaptan, M., Gülyüz, E., 2019. Relationship between the anisotropy of magnetic susceptibility and development of the Haymana Anticline, Central Anatolia (Turkey). Turk. J. Earth Sci. 28, 103–121.
Pares, J.P., Van Der Pluijm, B.A., Dinarès-Turell, J., 1999. Evolution of magnetic fabric during incipient deformation of mudrock (Pyrenees, northen Spain). Tectonophysics 307, 1–14.
Pearce, J.A., Bender, J.F., De Long, S.E., Kidd, W.S.F., Low, P.J., Güner, Y., Saroglu, F., Yilmaz, Y., Moorbath, S., Mitchell, J.G., 1990. Genesis of collision volcanism in Eastern Anatolia, Turkey. J. Volcanol. Geotherm. Res. https://doi.org/10.1016/0377-0273(90)90018-B.
Sağlam, A., 2003. Van Gölü Doğusu ve Güneydoğusunda Yüzeyleyen Van Formasyonunun Statigrafisi, Paleontolojisi, ve Çökelme Ortamları. Yüzüncü Yıl Universitesi.
Sagnotti, L., Faccenna, C., Funiciello, R., Mattei, M., 1994. Magnetic fabric and structural setting of Plio–Pleistocene clayey units in an extensional regime: the Tyrrhenian margin of central Italy. J. Struct. Geol. 16, 1243–1257.
Sancay, H., Batı, Z., Işık, U., Kırıcı, S., Akça, N., 2006. Palynomorph, Foraminifera, and Calcareous Nannoplankton Biostratigraphy of Oligo–Miocene Sediments in the Muş Basin, Eastern Anatolia, Turkey. Turkish Journal of Earth Sciences 15, 259–319.
Scheepers, P.J.J., Langereis, C.G., 1994. Paleomagnetic evidence for counter-clockwise rotations in the Southern Apennines fold-and-thrust belt during the late Pliocene and middle Pleistocene. Tectonophysics 239, 43–59.
Sengor, A.M.C., Gorür, N., 1985. Strike-Slip Faulting and Related Basin Formation in Zones of Tectonic Escape: Turkey as a Case Study. In: Biddle, K., Christie-Blick, N. (Eds.), Strike-Slip Deformation, Basin Formation, and Sedimentation. 37. Special Publications, SEPM Society for Sedimentary Geology, Tulsa, pp. 227–264.
Şengör, A.M.C., Yılmaz, Y., 1981. Tethyan evolution of Turkey: a plate tectonic approach. Tectonophysics 75, 181–241.
Şengör, A.M.C., Özeren, S., Genç, T., Zor, E., 2003. East Anatolian high plateau as a mantle-supported, north-south shortened domal structure. Geophys. Res. Lett. 30, 8045. https://doi.org/10.1029/2003GL017858.
Sönmez, M., 2004. Arapgir (Malatya) güneybatısındaki alanın stratigrafik ve tektonik özellikleri (Phd. Thesis). F.Ü Fenbilimleri Enstitüsü.
Soto, R., Larrasoaña, J.C., Arlegui, L.E., Beamud, E., Oliva-Urcia, B., Simón, J.L., 2009. Reliability of magnetic fabric of weakly deformed mudrocks as a palaeostress indicator in compressive settings. J. Struct. Geol. 31, 512–522. https://doi.org/10.1016/j.jsg.2009.03.006.
Soytürk, N., 1973. Murat Baseni Jeolojisi ve Hidrokarbon Olanakları. TPAO Arama Grubu Raporu, No. 791.
Türkmen, İ., Taşgın, C., Avşar, N., Aksoy, E., 2011. Sedimentological characteristics of Alibonca Formation (Upper Oligocene-Lower Miocene) near Arapgir-Yoncalı area (Malatya). Yerbilimleri 32, 235–254.
Yılmaz, Y., 1993. New evidences and model on the evolution of the southeast Anatolian orogen. Geol. Soc. Am. Bull. 105, 251–271.
Zhang, Z., Xiao, W., Majidifard, M.R., Zhu, R., Wan, B., Ao, S., Chen, L., Rezaeian, M., Esmaeili, R., 2017. Detrital zircon provenance analysis in the Zagros Orogen, SW Iran: implications for the amalgamation history of the Neo-Tethys. Int. J. Earth Sci. 106, 1223–1238.
Zijderveld, J.D.A., 1967. A.c. demagnetisation of rocks: analysis of results. In: Collinson, D.W. (Ed.), Methods in Palaeomagnetism. Elsevier, Amsterdam, pp. 254–286.
Zoetemeijer, R., Cloetingh, S., Sassi, W., Roure, F., 1993. Modelling of piggyback-basin stratigraphy: record of tectonic evolution. Tectonophysics 226, 253–269.